CONFERENCE PRE-PRINT

NON-INDUCTIVE PLASA START-UP USING ELECTRON BERNSTEIN WAVE MODE-CONVERTED FROM ELECTRON CYCLOTRON WAVE LAUNCHED FROM HIGH-FIELD SIDE ON SPERICAL TOKAMAK, QUEST

¹ K.HANADA, ²J.ZHOU, ²S.KOJIMA*¹, ²T.MURAKAMI*², ¹T.ONCHI, ¹H.IDEI, ¹T.IDO, ¹R.IKEZOE, ¹M.HASEGAWA, ¹Y.NAGASHIMA, ³K.KURODA, ⁴M.OYA, ⁵T.SHIKAMA ¹K.KONO, ¹S.KAWASAKI, ¹T.NAGATA ¹A.HIGASHIJIMA, ¹S.SHIMABUKURO, ¹I.NIIYA, ¹I.SEKIYA, ¹K.NAKAMURA, ⁶A.EJIRI ⁵S.MURAKAMI, ⁷X.GAO, ⁷H. Q. LIU, ⁷J. QIAN, ⁷Y. X. JIE, ⁸R. RAMAN

- ¹ Research Institute for Applied Mechanics, Kyushu University, Kasuga, Japan.
- ² Interdisciplinary Graduate School of Engineering Sciences, Kyushu University, Kasuga, Japan.
- ³ Japan Coast Guard Academy, Kure, Japan.
- ⁴ Faculty of Engineering Sciences, Kyushu University, Kasuga, Japan.
- ⁵ Department of Nuclear Engineering, Kyoto University, Kyoto, Japan.
- ⁶ Graduate School of Frontier Sciences, University of Tokyo, Kashiwa, Japan
- ⁷ ASIPP, China.
- ⁸ University of Washington, Seattle, WA, USA.
- *1 Present address: National Institutes for Quantum Science and Technology, Naka, Japan
- *2 Present address: Hitachi High-Tech Corp.

Email: hanada@triam.kyushu-u.ac.jp

Abstract

It is a crucial issue how to start-up plasma under insufficient inductive magnetic flux particularly in spherical tokamaks (STs). Electron cyclotron wave (ECW) injection is a promising candidate for magnetic flux consumption. In QUEST (Q-shu University experiments with steady state spherical tokamak), high field side (HFS) launch of the ECW X-mode has been performed to resolve the issue. The ECW X-mode approaches to the upper hybrid resonance (UHR) and is efficiently converted into electron Bernstein wave (EBW). The absorbed EBW near the 1st electron cyclotron resonance (ECR) could generate a closed flux surface (CFS) with a relatively high density of $(\omega_{pe}/\omega)^2 \sim 1$, here ω_{pe} and ω denote plasma frequency and injected ECW frequency, respectively. By changing B_T and B_R directions, the direction of part of plasma current, I_P in the open flux surface (OFS) was reversed, which is clear evidence for EBW current drive. The result was qualitatively explained by a ray-tracing calculation in the OFS. Some of anti-equilibrium current was observed, which might be useful to concentrate plasma current profile through cancellation of the pressure driven current, resulting in generation a CFS.

1. INTRODUCTION

Plasma current start-up is commonly recognized as a primary issue in tokamaks. The issue is particularly severe in the case of spherical tokamaks (STs), where there is insufficient space for a central solenoid (CS) in the central region of the torus. Plasma current start-up in the assistance with electron cyclotron wave (ECW) is a promising way to resolve the issue. However, most of the present STs have a higher dielectric constant than conventional tokamaks, making it difficult for the ECW to propagate into high-density plasma. As a result, generated plasmas are likely to be limited within relatively low density, which are not a suitable target of DT reactive plasmas. Electron Bernstein wave (EBW) is a promising candidate in this circumstance, because EBW has the capability for effective plasma start-up due to its inherent immunity to plasma density limit. In addition, EBW has good heating/current drive (CD) efficiency even in low-temperature plasma. EBW functions not only in the plasma start-up phase but also in the flat-top phase. In fact, the STEP fusion reactor being designed in the UK will use EBW as the plasma heating and current drive (CD) actuator for the flat-top DT plasma [1]. However, the characteristics of EBW in the plasmas are considerably more complex than ECW, as will be discussed later, and their understanding is further complicated by rapid plasma-parameter changes expected during the start-up phase. This clearly indicates the importance of EBW researches in ST plasma start-up.

Experiments of plasma start-up using EBW has been conducted in several STs [2-4]. The application of EBW to ST start-up was performed in LATE [2]. Antennas located in the low field side (LFS) for both 2.45 GHz and 5 GHz were used. In the experiment, the presence of EBW assist was supposed, because a significant high density of $(\omega_{pe}/\omega)^2 > 1$ was achieved, here ω_{pe} and ω denote plasma frequency and injected ECW frequency, respectively. During the rapid start-up phase of LATE plasmas, well-developed energetic electrons exceeding the runaway velocity were observed, suggesting the existence of a driving force that overcomes the inductively

induced retarding electric field [5]. Since only 2.45GHz ECW was injected as a driving source, high N_{II} EBW was the only possible candidate, here N_{II} denotes refractive index along with magnetic field line. Evidence of EBW was obtained by a direct measurement using a probe array insertion into an over-dense electron cyclotron resonance (ECR) plasma generated by obliquely injected ECW O-mode of 2.45 GHz from the LFS, but no closed flux surface (CFS) was formed [6]. A ST start-up using EBW was demonstrated in MAST, where 100 kW of ECW power injection generated a plasma current of 17 kA [3]. With assisted by loop voltage induced by vertical field, up to 33kA of plasma current was successfully obtained. A dedicated mirror for mode conversion from ECW O-mode launched from the LFS to ECW X-mode was located on the inner wall of the high field side (HFS) in the experiment. The dedicated mirror was previously used in WT-3 tokamak [7]. The ECW X-mode was propagating from the HFS and was effectively converted to an EBW in the vicinity of the upper hybrid resonance (UHR). Ray-tracing and quasilinear Fokker-Planck modelling could reconstruct the experimental results. This indicated the EBW was available to ST start-up. In QUEST, plasma start-up with EBW through a modeconversion from HFS launched ECW has been conducted with a dedicated waveguide and antenna [4]. The HFS launched ECW is expected to convert into EBW effectively and the mode-converted EBW is completely absorbed in the vicinity of 1st electron cyclotron resonance (1st ECR) layer. A quantitative analysis using GENRAY code [8,9] has been performed under the QUEST parameters [10]. The calculation indicates that increasing the electron temperature, T_e, induces a mechanistic shift from collisional damping to electron cyclotron damping, resulting in EBW-driven CD (EBWCD) with sufficient CD efficiency to form CFS even in the O-X-B scenario. However, in actual ECW injection, the beam waist may expand due to limitations in antenna size, so we decided that the X-B scenario from HFS was more suitable for the experiment. In fact, the formation of CFS has been obtained by HFS X-B scenario [11]. It should be noted that the GENRAY code is applicable to calculate current drive efficiency only in a CFS, so we have developed a ray-tracing code that can be used for open flux surfaces (OFSs). The sideband observation suggested that EBW was induced due to X-B scenario in this experiment [12].

2. Experimental apparatus and dedicated experimental set-up

The experiments have been performed in QUEST (Q-shu University Experiment with Steady State Spherical Tokamak), which has major and minor radii of R=0.68m, a=0.4m, respectively and the aspect ratio R/a = A = 1.7. It is equipped with a 16 turns toroidal magnetic field coil, which is capable of generating toroidal magnetic field, B_T , up to 0.25T CW at R=0.64m. Each turn connects to the next on the top side of the coil, resulting in a significant vertical field, B_V , in the plasma region. To cancel the B_V , a vertical magnetic field coil with a coil current flowing in the opposite direction is placed nearby, resulting in a slight horizontal magnetic field, B_R , in the plasma region. The B_R coil with a coil current of about 20 A can eliminate the B_R on the midplane, but it cannot completely eliminate the B_R throughout the plasma region. It should be noted that the residual B_R has a non-negligible effect on the plasma in this experiment. If the top side of the B_R coil current is oriented clockwise when viewed from the top, we refer to it as negative B_R in this paper. If B_T is oriented clockwise when viewed from the top, we refer to it as B_T (CW). The residual B_R induced by B_T (CW) is eliminated by the negative B_R coil current. If I_P is oriented clockwise when viewed from the top, we refer to it as negative I_P . Two pairs of the vertical field coil are used to make a plasma equilibrium in this experiment, and if the coil current of the B_V coil is oriented clockwise when viewed from the top, we refer to it as B_V (CW). A positive I_P can be in equilibrium with B_V (CW).

The ECW power is supplied through a dedicated waveguide, a vacuum window, and an antenna. The waveguide is made of Cu on the vacuum vessel side and Cu and Al on the atmosphere side. A special flange for vacuum sealing was temporarily installed at the QUEST port, and a total of two waveguides were installed as shown in Fig. 1. The vacuum window consisted of a round sapphire plate and a copper water jacket. The power that could be passed at 8.2 GHz was 25 kW each for short pulses only. To prevent arcing, the window was placed midway through the waveguide in the vacuum side, avoiding the location of the ECR layer. No cooling water was provided in this experiment, limiting the available pulse length to less than 1 second. As shown in Fig. 1, multiple supports for the waveguide were installed and the antennas were attached to the end of the waveguide. Due to the limited antenna size, the power radiation distribution is significantly expanded by approximately 60°in both the toroidal and poloidal directions [4]. The poloidal and toroidal expansions give rise to cancellation of I_P and different propagation due to the wave refection around the left-hand cut off (L-cutoff) because of N_{\emptyset} dependence on L-cutoff, respectively. Here, N_{\emptyset} denotes reflective index to the toroidal direction. The details would be discussed later.

Several diagnostics to observe the plasma responses are utilized. Magnetic structure was monitored with 64 flux loops distributed on the surface of the vacuum vessel and plasma current distribution was reconstructed using a developed model calculation [13]. In this paper, the flux loops on the CS cover were mainly used as shown in Fig.

2. The magnetic flux signals from the flux loops were acquired with 8 oscilloscopes with sampling rate of 500 kHz and then the signals were time integrated to obtain the magnetic fluxes at the position. Because the signal drifted with time, we used linear fitting just before and after each discharge to remove the drift component. The technique was also used for plasma current measurement. The locations of the flux measurement and the antennas are schematically illustrated in Fig. 2. Electron density profile is extremely important in this research and measured with an insertion probe, an interferometer, and Thomson scattering diagnostics. The insertion probe was used in a short pulse within 20ms, but the time-space resolutions was better than the others. The n_e values derived from the probe signal was calibrated with Thomson scattering diagnostics [14].





Fig. 1 Left: A photograph of the dedicated waveguides and the flange from the vacuum side of the vacuum vessel of QUEST. Right: A photograph of the dedicated antennas and antenna covers. The covers were made of tungsten.

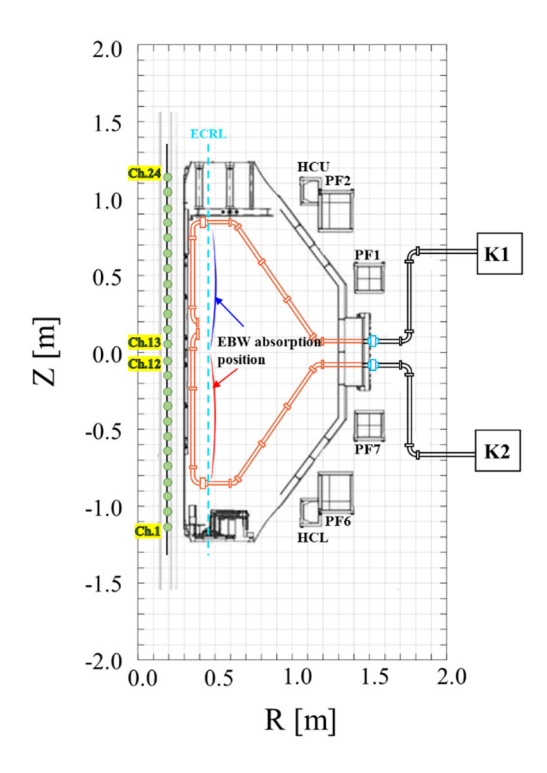


Fig. 2 A poloidal cross-sectional view of QUEST in the dedicated experiments. There are 24 flux loops on the CS cover and two waveguides and the antennas with the guard. K1 and K2 represents two klystrons for 8.2 GHz, 25 kW each. The ECR layer is indicated by the vertical dotted line and the expected absorption areas for EBW are also illustrated with red and blue areas. The different colour means the reversed I_P direction. The magnetic flux loops on the inner vessel are located as marked by green circles. A pair of PF2 and PF6 coils are connecting in

series to generate the B_V with a positive n-index. A pair of PF1 and PF7 coils are connecting in series to generate the B_V with a negative n-index. The pair of HCU and HCL coils are also connecting in series to generate the B_R .

3. Experimental Results

The experiments were performed on QUEST. The magnetic configurations in the experiment are listed in the table 1. It should be noted that the EBW driven current direction is depending on both B_T and B_R directions, since N_{\parallel} at the vicinity of 1st ECR for the EBW is expressed by an approximated equation, $N_{\parallel} \cong N_{\phi}/R + N_R B_R/B$, where B is the absolute strength of magnetic field. In addition, N_R of the EBW at the vicinity of 1st ECR is considerably high, so the current drive direction is dominantly determined by the second term $N_R B_R/B$. The EBWCD direction is inversed by the sign of B_R . As a result, opposite EBWCD currents are expected to be driven on the top and bottom sides due to the reversed sign of B_R . This indicates that B_R induced by the horizontal magnetic field coil may be utilized to modify the current profile by controlling the B_R structure. When the direction of B_T is inverted, the sign of N_{\parallel} is not change, but because the magnetic field direction is inverted, the EBWCD direction is also inverted. When starting a plasma, the direction of the equilibrium current must be taken into consideration, since the plasma current that creates equilibrium is more important and meaningful than the anti-equilibrium current. The equilibrium current direction is always determined by the direction of B_V . It should be noted that the equilibrium area is always located in the top in B_T (CCW) as denoted in the table 1.

	B_T	B_V	I_P	Тор	Bottom
Case 1	CCW	CCW	CW	equilibrium	anti-equilibrium
Case 2	CW	CCW	CW	anti-equilibrium	equilibrium
Case 3	CW	CW	CCW	anti-equilibrium.	equilibrium
Case 4	CCW	CW	CCW	equilibrium	anti-equilibrium.

Table 1: List for the magnetic structure in the experiments.

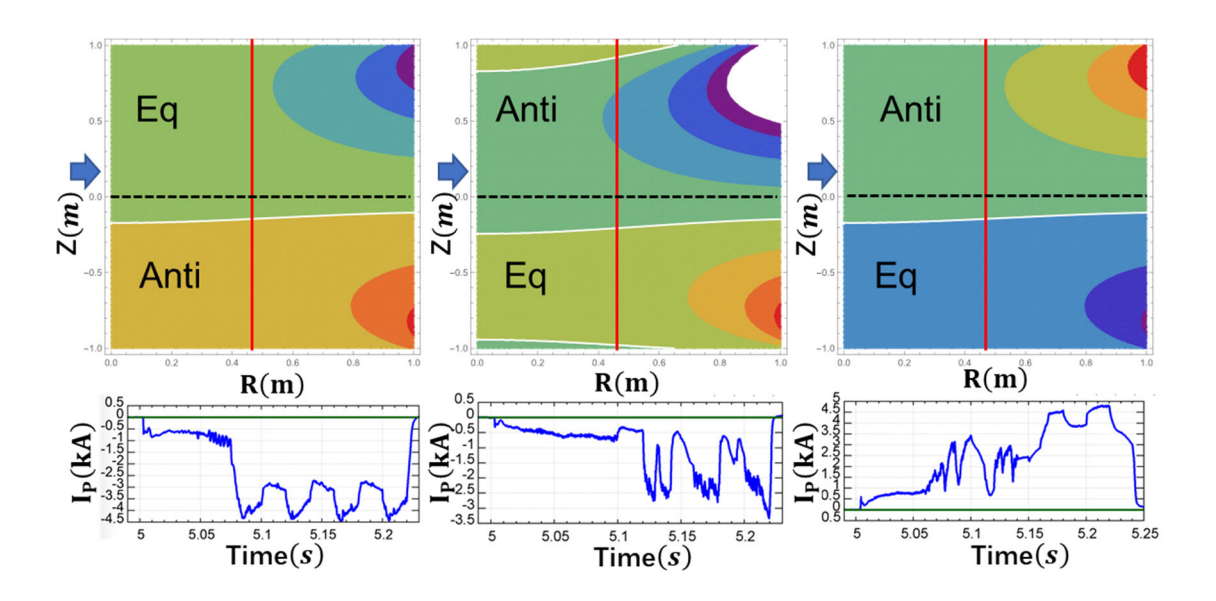


Fig. 3 The B_R conditions for various B_T and I_P direction on the map of R=0~1.0m (vertical axis) and Z=1~1m (horizontal axis). The white lines denote $B_R = 0$ boundary. Time evolutions of I_P are also plotted. "Eq" and "Anti" region in the diagram denotes EBWCD direction for equilibrium and anti-equilibrium. The dotted line indicates the midplane. The B_R structure was modified by the error field from the toroidal coil. The ECR layer was located at the vertical red line. The ECW power was modulated from 40kW to 20kW three times from 5.1s. It should be noted that the injection antenna was located at the top side marked by a blue arrow in each diagram.

The case 1 was performed as a standard QUEST operation. The case 2 was conducted as an investigation of the pure B_T inversion effect. There are three candidates to drive I_P in the OFS: EBWCD, ECCD, and pressure driven current. Only the direction of EBWCD is expected to reverse in the case of the B_T reversal. The case 3 was planned to confirm the B_V reversal effect, where the directions of both the ECCD and the pressure-driven current are reversed. Finally, the case 4 was performed to complete the comparison of all magnetic structures. The B_R values varied in cases 1 to 3. Each pulse length was limited by 0.25 s and the stability of the plasma start-up was confirmed by power modulation.

The 2-dimentional (2D) B_R conditions on the map of R=0~1.0m (vertical axis) and Z=-1~1m (horizontal axis) are illustrated in Fig. 3. The case 1 is denoted in the top-left diagram. The B_R value in the top side was negative (The B_R was directed to the HFS (cold color).) and was positive in the bottom side (warm color). The EBWCD direction in the top side was expected to be directed to CW. The direction of I_P was directed to CW, that is inverted to the B_V coil current direction, so that the EBWCD worked to make an equilibrium current. While, in the bottom side, the EBWCD direction was inverted due to the positive B_R , so it drove an anti- equilibrium current. The horizontal coil current, I_{hor} , was just 50A (-20A was necessary to partially eliminate the error field generated by the toroidal field coil.) and plasma start-up was successfully demonstrated as shown in the left bottom diagram in Fig. 3. While, the plasma start-up was failed in CW at $I_{hor} = 90A$ (20A was needed to cancel toroidal coil effect) in the case 2 as shown in the middle diagrams. In addition, the plasma start-up was not stable in CW at $I_{hor} = 90A$ in the case 3 as shown in the right diagrams. The magnetic structures are selected to adjust the $B_R = 0$ boundary expressed by white lines in Fig. 3. This indicated that the plasma start-up was smoothly established when the equilibrium zone was located in front of the injection antenna. This suggests that the EBWCD dominantly worked in the plasma start-up phase, because the direction of both ECCD and pressure driven current is depending on only the I_P direction, not the B_T direction.

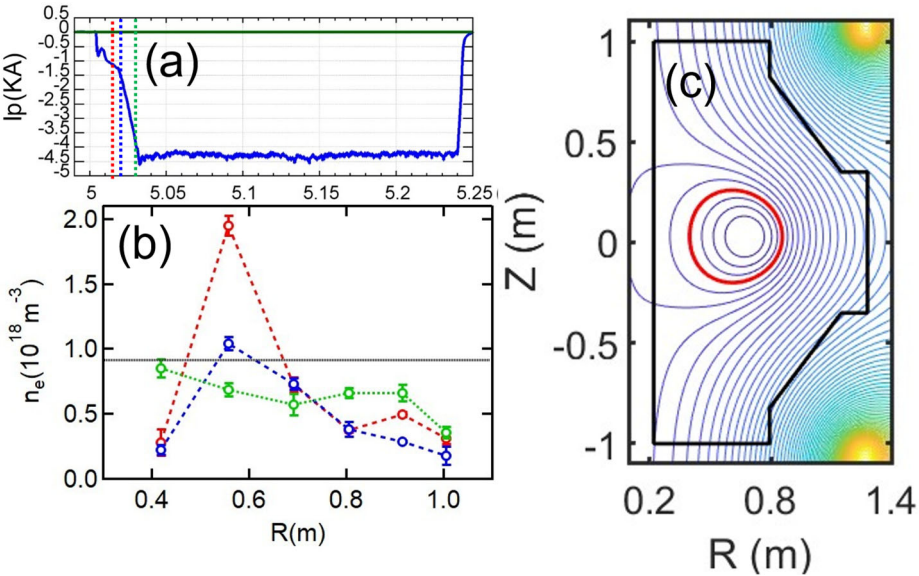


Fig. 4 The time evolution of I_P in the case that the equilibrium I_P region located in the bottom area (B_T CW), is plotted in the diagram (a). Three lines denote the timing of n_e measurement with Thomson scattering. The measured n_e profiles are plotted in the diagram (b). The line color corresponds to the time indicated in the diagram (a). A horizontal line represents $\left(\omega_{pe}/\omega\right)^2=1$, where ω_{pe} and ω denote plasma frequency and injected ECW frequency, respectively. Magnetic flux surface reconstructed by an equilibrium code at 5.05s is shown in the diagram (c). The red circle shows the LCFS. An antenna cover shown in Fig. 2 was positioned at R=0.4m.

Even in the cases 2 and 3, the smooth plasma start-up could be achieved by the B_R structure control using the horizontal coil current as shown in Fig. 4. In the magnetic structure of B_T (CW), B_V (CCW), I_P (CW) and $I_{hor} = -20A$, I_P was smoothly ramp-up and reached up to more than 4 kA as denoted in Fig. 4(a). The equilibrium current was expected to be mainly in the bottom side, but the boundary of $B_R = 0$ was slightly expanded to the top side due to the application of I_{hor} . The time evolution of the n_e profile is plotted in Fig. 4(b). It should be noted that $\left(\omega_{pe}/\omega\right)^2 \approx 2$ was achieved at the beginning of the discharge. The tendency of high n_e just after the plasma initiation was commonly observed in the HFS launch experiment on QUEST [14].

The high n_e corresponding to $(\omega_{pe}/\omega)^2 \approx 2$ played an essential role in plasma start-up feature through the appearance of L-cutoff in front of the injection antenna as described later. The peak n_e was decreasing with time and a flat n_e profile was achieved when the I_P was almost constant.

The most apparent feature in the HFS launched experiments was the formation of a CFS as shown in Fig. 4(c), although CFS was never seen in the case of the LFS launch in the same magnetic configuration and injection power. Actually, at the time of 5.05s, the CFS had been formed and $\left(\omega_{pe}/\omega\right)^2 \cong 1$ was achieved at the injection power of 40 kW as shown in Fig 4(b) and (c). Before the CFS formation, the value of n_e was satisfied with $\left(\omega_{pe}/\omega\right)^2 \cong 2.0$. A Langmuir probe could be inserted into the plasma, and the details of n_e and T_e profiles and their time-evolutions could be obtained within 20ms at the mid-plane [14]. Assuming constancy of these parameters on the flux surface, calculations that could trace the ECW and EBW rays for the MC and subsequent EBW propagation and absorption are allowable. The 2D situation is illustrated under the assumption in Fig. 5.

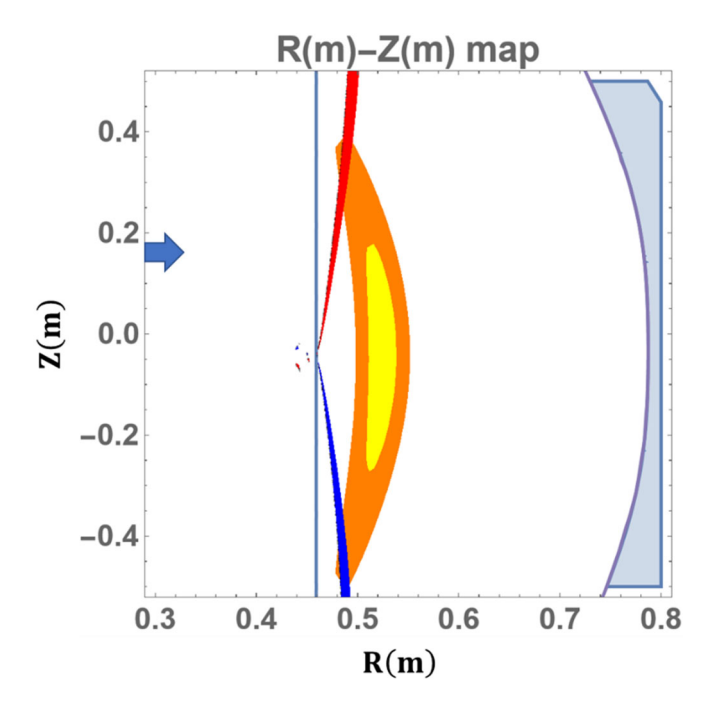


Fig. 5 Typical experimental situations are illustrated on a R-Z map. A vertical blue line, orange and yellow regions denote 1st ECR and L-cutoff at the case of $(\omega_{pe}/\omega)^2 \cong 2$ for $N_0=0.1$ and 0.2 of ECW, respectively. A purple line, red and blue regions indicate UHR, EBW deposition regions to drive anti-equilibrium I_P (red) and equilibrium I_P (Blue) in the case of B_T (CW). The area not propagating the ECW is expressed by a blue shadow, where is the area between UHR and R-cutoff for ECW X-mode. The injection antenna was located at Z=0.17m.

The red and blue areas correspond to the deposition area of the EBW, where the equilibrium (red) and antiequilibrium (blue) current drive are expected by EBWCD, respectively [15]. This illustration clearly indicates that the wave propagation and absorption are significantly affected by the high density such as $(\omega_{pe}/\omega)^2 \cong 2.0$.

Using n_e and T_e profiles measured with the insertion probe [13] and Thomson scattering, the wave propagation and mode conversion characteristics are investigated by a newly developed ray-tracing code. The results were compared with the flux loop signals measure in the experiments as shown in Fig. 6. As the ECW is expanded by approximately 60° in both the toroidal and poloidal direction [4], the rays with various poloidal angles are calculated. In the case of high n_e of $(\omega_{pe}/\omega)^2 \cong 1.8$, the ECW ray passes through an ECR without significant absorption, because the absorption of ECW X-mode is week in the case of $(\omega_{pe}/\omega)^2 > 1$ [13]. However, in the case of high n_e of $(\omega_{pe}/\omega)^2 \cong 1.8$, the L-cutoff prevents ECW X-mode from propagating to the LFS and the ECW reflected back to the HFS as shown in Fig. 6(a). The ECW was likely to suffer from multiple reflections between the L-cutoff with the center stack. Then the ECW passes through accessible areas as shown in Fig. 6(a) (see one green ray is drown in Fig. 6(a) as a reference). The passed ECW gradually bends and eventually turns

back towards HFS at the vicinity of UHR. The ECW was effectively converted into an EBW. The EBW was absorbed in the blue region, where the EBWCD drove the anti-equilibrium current. Because the raytracing was done for the condition of B_T (CCW), the equilibrium current was expected to be driven by the EBW on the top side, and the anti- equilibrium current, which is cancelled by the pressure-driven current, was expected to be driven on the bottom side in the simulation. In the high n_e , the simulation indicates the equilibrium current could not be expected by EBWCD. In the case of medium n_e of $(\omega_{pe}/\omega)^2 \cong 1.6$ (see Fig. 6(b)), most of rays can reach UHR. The group velocity of the wave slows down and mode conversion to EBW takes place. The signal measurements with magnetic flux loops showed that the equilibrium current was present on the top side and vanished on the bottom side as denoted by red circles shown in Fig 6(c). As the effect of pressure driven current was included in the experimental data, the anti-equilibrium current by EBWCD cancelled out the pressure driven current in the bottom side. The experimental results match with the raytracing calculation. This cancellation effect worked well by creating current concentration that played an essential role in the formation of CFS. Thus, EBWCD in both directions functioned to form a CFS. The HFS launched mode conversion process is predictable when 2D n_e and T_e profiles are obtained, compared with the other mode conversions from ECW to EBW such as OXB and XB of LFS launch. This is why we decided to conduct experiments by installing a new dedicated antenna in the HFS on QUEST.

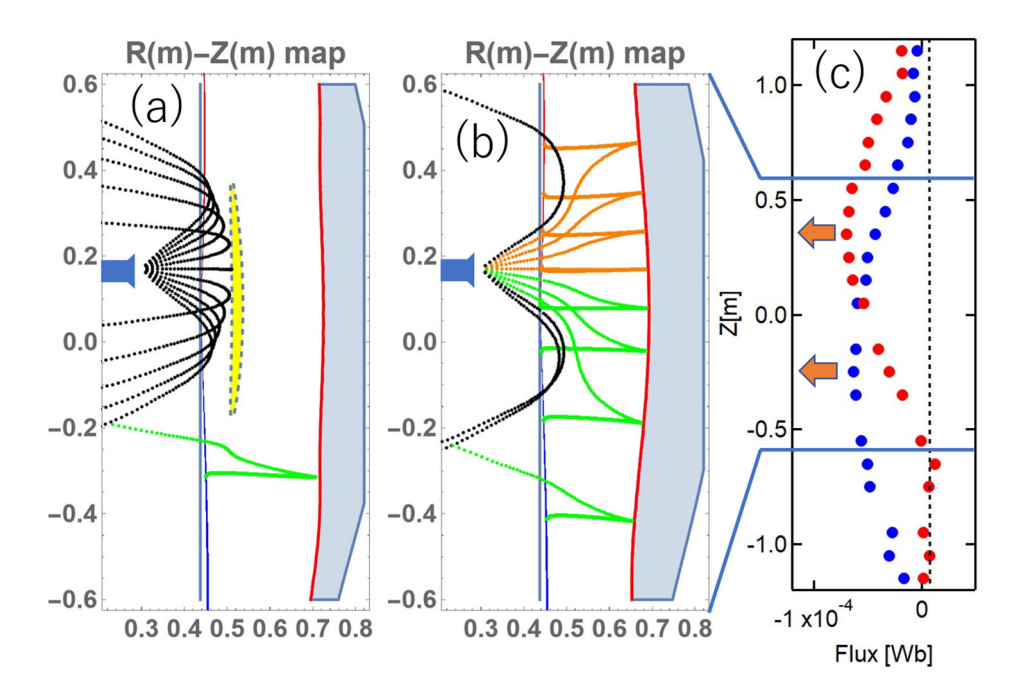


Fig. 6 (a) Typical conditions for EBW for the case of $\left(\omega_{pe}/\omega\right)^2 \cong 1.8~B_T$ CCW for N_0 =0.1 at the head of the antenna (see the blue mark) are illustrated on a R-Z map. Vertical blue and red lines denote 1st ECR and UHR. The yellow region indicates L-cutoff for N_0 =0.1. Red and blue regions show EBW deposition regions to drive equilibrium I_P (red) and anti-equilibrium I_P (blue). The black rays are ECW reflected by L-cutoff and a green ray indicates a reflected ECW at the center stack. The mode-converted EBW is absorbed at the vicinity of 1st ECR layer. (b) Typical conditions for $\left(\omega_{pe}/\omega\right)^2 \cong 1.6$. The orange and green rays show wave trajectory to drive equilibrium I_P and anti-equilibrium I_P , respectively. (c) I_P induced magnetic flux (red B_T CCW: blue B_T CW) on the center stack measured with flux loops as a function of Z position. The left-directed arrow denotes equilibrium I_P direction.

We would like to confirm the engineering EBWCD efficiency, η_{CD} in the OFS and CFS configurations. In the case of OFS, the estimation is a little complicated, because equilibrium and anti-equilibrium I_Ps are cancelled out in total. The substantial EBWCD efficiency should be estimated by adding both I_Ps . A TF inversion experiment has been conducted to obtain the sum of both I_Ps . Under the assumption of the same pressure driven current in both cases, the sum of both I_Ps is determined to be approximately 0.5-0.6 kA by a current reconstruction technique [13] in the case of $P_{RF} = 40kW$. The value of η_{CD} is about 0.015 A/W, which is comparable to that in ECW X-mode at 1st ECR expected in future fusion pilot plant, STAR at low density and

temperature region [16]. The value of η_{CD} in the case of CFS was $0.1 \, A/W (4kA/40kW)$ even in the low T_e region less than 100 eV. It should be noted that the anti-equilibrium I_p may be driven by EBWCD even in the CFS, and a part of equilibrium I_p may be cancelled out. The value of η_{CD} (0.1 A/W) in the CFS is higher than that in STEP (0.03 A/W at 98GHz, $T_e = 4keV$) calculated with fully relativistic EBW simulation [17]. This observation in QUEST provides a bright outlook for the plasma current start-up in future ST-based fusion reactors, if we can solve the problem of having to install an antenna in the narrow HFS area. Focusing the wave is also important to minimize the anti-equilibrium I_p .

4. Conclusion

In QUEST, the experiments were performed to plasma start-up with ECW X-mode using the dedicated antenna for the HFS launch. The ECW was propagating to the LFS and passing through the 1st ECR layer, because the ECW absorption was predicted to be slight in the high n_e region such as $(\omega_{pe}/\omega)^2 > 1$. The passed ECW approached the UHR, was converted into the EBW. The EBW was effectively absorbed near 1st ECR layer and drove I_p , resulting in the formation a CFS. The clear evidence of EBWCD could be obtained by changing B_T and B_R directions. Four magnetic configurations were conducted to confirm the EBWCD effect. The direction of the driven current is reversed depending on the directions of B_T and B_R , which is characteristic of EBWCD, not ECCD or pressure-driven current. The results were qualitatively agreed with the ray-tracing calculation. The B_R scan with the horizontal field coil were performed. The results indicated that the B_R control was useful to obtain the smooth plasma start-up. In conclusion, EBWCD played an important role in plasma start-up in the ECW X-mode HFS launch. The most notable feature of the HFS launch was the formation of CFS, but the CFS has never been realized in the LFS launch with the same magnetic field configuration. This indicated that the HFS launch played an essential role in effective mode conversion into EBW and the EBWCD sufficiently functioned in the CFS formation. In particular, the observed engineering current drive efficiency even in the OFS condition was comparable to that expected in future fusion pilot plants.

ACKNOWLEDGEMENTS

One of the authors (K. Hanada) sincerely appreciate Prof. M. Ono for his accurate suggestions for the experiment and analysis. Funding: This work was supported by a Grant-in-Aid for JSPS Fellows (KAKENHI Grant Number 16H02441, 21H04456, 24656559) and the NIFS Collaboration Research Program (NIFS05KUTR014, NIFS13KUTR093, NIFS13KUTR085, and NIFS14KUTR103). This work was also supported in part by the Collaborative Research Program of the Research Institute for Applied Mechanics, Kyushu University.

REFERENCES

- [1] Tholerus, E., et al. Nucl. Fusion **64** 106030 (2024).
- [2] Maekawa, T., et al., Nucl. Fusion 45 (2005) 1439–1445.
- [3] Shevchenko, V.F., et al., Nucl. Fusion 50, 22004 (2010).
- [4] Elserafy, H., et al., Plasma Phys. Contr. Fusion. 26 035018 (2020).
- [5] Uchida, M., et al. Phys. Rev. Lett. 104 065001 (2010).
- [6] Guo, X., et al., Plasma Phys. Control. Fusion 64 035008 (2022).
- [7] Maekawa, T., et al., Phys. Rev. Lett. 86 3783 (2001)).
- [8] Smirnov, A.P., Harvey, R.W., Bull. Am. Phys. Soc. 40, 1837, abstract 8p35 (1995).
- [9] Mazzucato, E., et al., Phys. Fluids 30, 3745 (1987).
- [10] Yoneda, R., et al., Plasma and Fusion Research, 13, 3402115 (2018).
- [11] Kojima, S., 2021 Doctor thesis, Kyushu University.
- [12] Kojima, S., Plasma and Fusion Research, 15, 2402063 (2020)
- [13] Zhou, J., et al., Evergreen. 11, 555-562 (2024).
- [14] Murakami, T., et al., Plasma Phys. Control. Fusion 66 115016 (2024).
- [15] Maekawa, T., et al., Plasma Phys. Control. Fusion 61 105017 (2019)
- [16] Ono, M., et al., Nucl. Fusion 64 086021 (2024).
- [17] Biswas, B., et al., Nucl. Fusion 65 016010 (2025).